Journal of Solid State Chemistry **162,** 63–68 (2001)
doi:10.1006/jssc.2001.9341, available online at http://www.idealibrary.com on IDEAL®

Theoretical Study of Possible Iridium Ditelluride Phases Attainable under High Pressure

S. Jobic and R. Brec

Institut des Matériaux Jean Rouxel, 2 rue de la Houssinière, BP 32229, 44322 Nantes Cedex 3, France

A. Pasturel

Laboratoire de Physique Numérique, CNRS, 25 avenue des Martyrs, BP 166, 38042 Grenoble, France

and

H.-J. Koo and M.-H. Whangbo[1]

Department of Chemistry, North Carolina State University, Raleigh, North Carolina 27695-8204

Received April 4, 2001; in revised form June 29, 2001; accepted August 2, 2001

We examined the feasibility of preparing new high-pressure polymorphs of $IrTe_2$ by determining the relative energies and unit cell volumes of known and hypothetical forms of $IrTe_2$ on the basis of first-principles electronic band structure calculations using the Vienna *ab initio* simulation package (VASP). The $IrTe_2$ polymorphs included in our analysis are three known phases, i.e., the polymeric CdI_2-type, pyrite-type, and monoclinic $IrTe_2$ phases, as well as four hypothetical phases, i.e., ramsdelite-type, pyrolusite-type, IrS_2-type, and marcasite-type phases. The charge balances of these $IrTe_2$ phases were analyzed by carrying out extended Hückel tight-binding electronic band structure calculations for the crystal structures optimized by VASP calculations. © 2001 Academic Press

1. INTRODUCTION

For transition metal tellurides the *p*-block bands of Te can overlap with the *d*-block bands of the transition metal and leads to electron transfer from the top of the *p*-blocks bands into the *d*-block bands. This electron depletion causes a shortening of Te ⋯ Te contacts because the top part of the Te *p*-block bands is antibonding between Te atoms (1). Thus many transition metal tellurides exhibit short Te ⋯ Te contacts intermediate between the Te–Te single-bond length of $(Te_2)^{2-}$ dimers and the $Te^{2-} \cdots Te^{2-}$ van der Waals contacts (2–8). A representative example showing the complexity of the redox competition between transition metal and Te is $IrTe_2$ (9), for which three different phases are known, i.e., the polymeric CdI_2-type, pyrite-type, and monoclinic $IrTe_6$ phases. The polymeric CdI_2-type phase consists of $IrTe_2$ layers in which adjacent $IrTe_6$ octahedra share only edges (Fig. 1a) (9, 10). In the pyrite-type $IrTe_2$ (Fig. 1b) adjacent $IrTe_6$ octahedra share only corners (11). The monoclinic $IrTe_2$ (Fig.1c) is made up of $IrTe_4$ single-octahedral chains (obtained by sharing trans edges of $IrTe_6$ octahedra) as well as Ir_2Te_6 double-octahedral chains (formed from two $IrTe_4$ chains sharing their octahedral edges) in the 1:1 ratio (11, 12). The pyrite-type and monoclinic $IrTe_2$ phases are obtained when a sample of the polymeric CdI_2-type $IrTe_2$ is subjected to pressure. Therefore it is of interest to question if it is possible to prepare other high-pressure polymorphs of $IrTe_2$.

We may consider several hypothetical $IrTe_2$ phases by analogy with the isostructural oxides and sulfides. The ramsdelite-type phase (Fig. 1d) consists of only corner-sharing Ir_2Te_6 double-octahedral chains, while the pyrolusite-type structure (Fig. 1e) has only corner-sharing $IrTe_4$ single-octahedral chains (13). In the IrS_2-type phase (Fig. 1f), single- and double-octahedral chains occur in the 2:1 ratio (14, 15). The marcasite-type phase (Fig. 1g) may be viewed as a pyrolusite-type structure with added Te–Te dimers between chains (13). In the present work we probe the feasibility of preparing these hypothetical polymorphs under pressure on the basis of first-principles electronic band structure calculations.

[1] To whom correspondence should be addressed. E-mail:whangbo@ncsu.edu.

0022-4596/01 $35.00

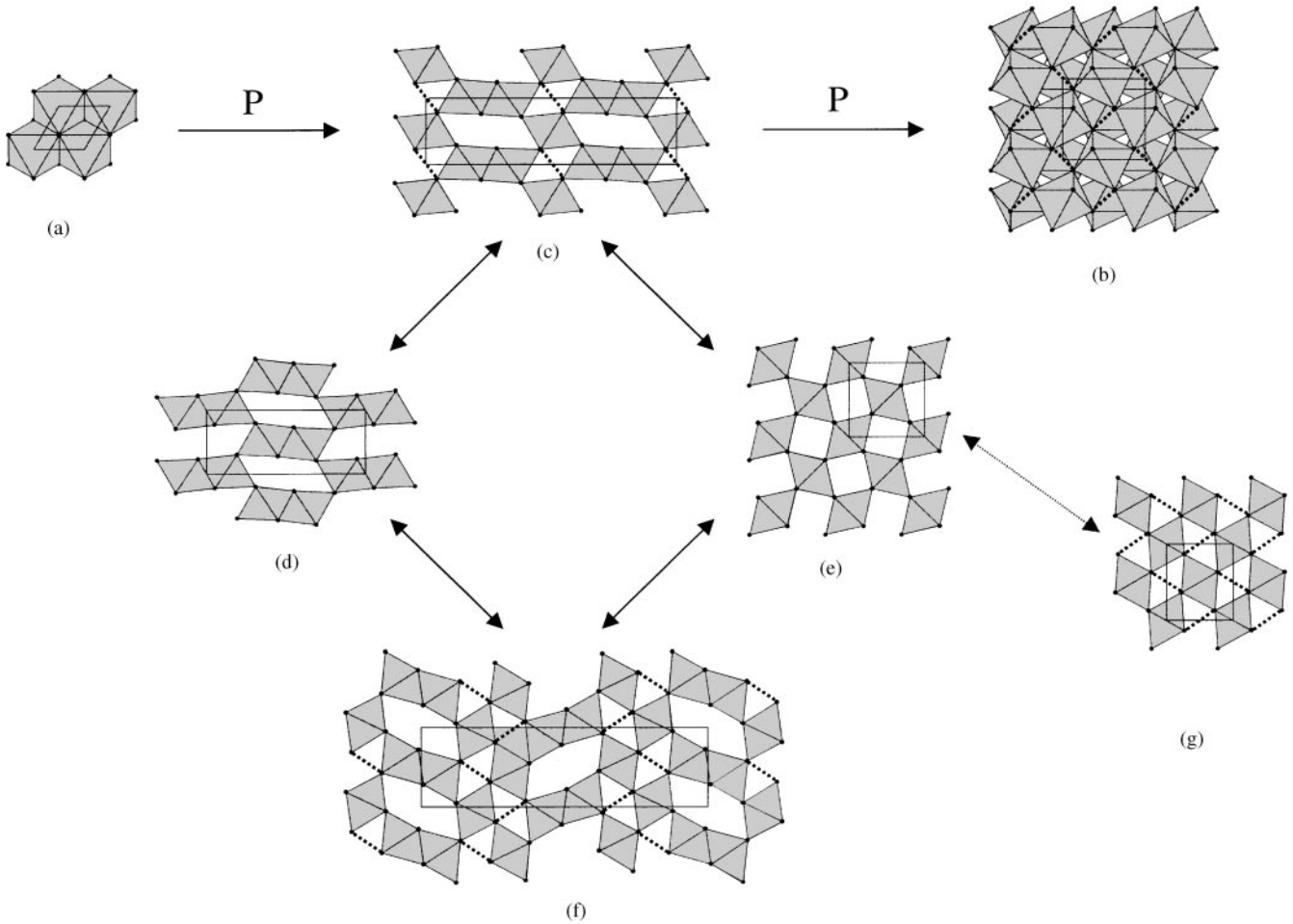

FIG. 1. Schematic projection views of some observed and hypothetical $IrTe_2$ phases: (a) A single $IrTe_2$ layer of the polymeric CdI_2-type phase along the direction perpendicular to the layer. (b) The pyrite-type phase. (c) The monoclinic phase along the direction of the $IrTe_4$ single-octahedral chains. (d) The ramsdellite-type phase along the direction of the Ir_2Te_6 double-octahedral chains. (e) The pyrolusite-type phase along the direction of the $IrTe_4$ single-octahedral chains. (f) The IrS_2-type phase along the direction of the $IrTe_4$ single-octahedral chains. (g) The marcasite-type phase along the direction of the $IrTe_4$ single-octahedral chains. The bold-dotted lines represent Te_2 pairs with Te–Te distances shorter than 3.1 Å.

2. COMPUTATIONAL DETAILS

The cell parameters and the atom positions of various $IrTe_2$ phases were optimized by performing electronic band structure calculations using the Vienna *ab initio* simulation package (VASP) (16). Since the details of this program package were described elsewhere (17–19), we briefly mention its essential characteristics. The VASP is based on the density functional theory within the local-density approximation and employs pseudopotentials. With the Te 5*s*/5*p* and the Ir 5*d*/6*s*/6*p* orbitals taken as valence orbitals the ultrasoft pseudopotentials were constructed using the Vanderbilt recipe (20, 21). We employed a finite temperature density functional approximation, an optimized mixing routine, and a conjugate gradient scheme. The integration in the Brillouin zone was performed on a set of special *k*-points determined by the Monckhorst–Pack scheme. All calculations were performed using the generalized-gradient approximation as proposed by Perdew and Wang (22).

The structural data of the real and hypothetical $IrTe_2$ phases determined by VASP calculations are summarized in Tables 1a–1g. For the observed $IrTe_2$ phases, the experimental values of the cell parameters and atom coordinates are also given in parentheses in Tables 1a–1c. The relative energies and unit cell volumes of these phases (per formula unit) determined by VASP calculations are listed in Table 2. In analyzing the charge balances of these compounds, population analysis is indispensable. In the present work we examined the charge balances by performing extended Hückel tight-binding band (EHTB) structure calculations (23, 24) for the crystal structures optimized by VASP calculations. The gross populations of the $IrTe_2$ phases calculated by the EHTB method are listed in Tables 3. The plots of the density of states (DOS) for the various $IrTe_2$

TABLE 1
Crystal Structures of Real and Hypothetical Phases of $IrTe_2$ Determined by VASP Calculations

(a) Polymeric CdI_2-type $IrTe_2$[a]
SG: $P\bar{3}m1$; $a = 3.9912$ (*3.9284*) Å, $c = 5.4709$ (*5.4049*) Å, $V = 75.47$ (*72.23*) Å^3
Atom coordinates: Ir (0, 0, 0); Te ($\frac{1}{3}$, $\frac{2}{3}$, 0.7489 (*0.7464*))

(b) Monoclinic $IrTe_2$[a]
SG: $C2/m$, $a = 20.1978$ (*19.9746*) Å, $b = 4.0713$ (*4.0016*) Å, $c = 5.4129$ (*5.3119*) Å, $\beta = 90.44°$ (*90.82°*), $V = 445.10$ (*424.54*) Å^3
Atom coordinates: Ir(1) (0.3405 (*0.3398*), 0, 0.0021 (*0.0027*)); Ir(2) ($\frac{1}{2}$, $\frac{1}{2}$, $\frac{1}{2}$); Te(1) (0.4557 (*0.4556*), 0, 0.7775 (*0.7754*)); Te(2) (0.2806 (*0.2809*), $\frac{1}{2}$, 0.7598 (*0.7545*)); Te(3) (0.3788 (*0.3804*), $\frac{1}{2}$, 0.2861 (*0.2802*))

(c) Pyrite-type $IrTe_2$[a]
SG: $Pa\bar{3}$, $a = 6.5547$ (*6.432*) Å, $V = 281.62$ (*266.10*) Å^3
Atom coordinates: Ir (0, 0, 0); Te (0.3672 (*0.362*), 0.3672 (*0.362*), 0.3672 (*0.362*))

(d) Ramsdelite-type $IrTe_2$
SG: $Pnma$, $a = 13.5116$ Å, $b = 4.0671$ Å, $c = 5.5275$ Å, $V = 303.75$ Å^3
Atom coordinates: Ir (0.1346, $\frac{1}{4}$, 0.9780); Te(1) (0.3081, $\frac{1}{4}$, 0.1998); Te(2) (0.9484, $\frac{1}{4}$, 0.7712)

(e) Pyrolusite-type $IrTe_2$
SG: $I4_2/mnm$, $a = 6.1472$ Å, $c = 4.2017$ Å, $V = 158.78$ Å^3
Atom coordinates: Ir (0, 0, 0); Te (0.3066, 0.3066, 0)

(f) IrS_2-type $IrTe_2$
SG: $Pnma$, $a = 22.9525$ Å, $b = 4.0789$ Å, $c = 6.4761$ Å, $V = 606.29$ Å^3
Atom coordinates: Ir(1) (0.0758, $\frac{1}{4}$, 0.5680); Ir(2) (0.3057, $\frac{1}{4}$, 0.5605); Te(1) (0.3635, $\frac{1}{4}$, 0.9230); Te(2) (0.6218, $\frac{1}{4}$, 0.5512); Te(3) (0.7594, $\frac{1}{4}$, 0.3112); Te(4) (0.9911, $\frac{1}{4}$, 0.2784)

(g) Marcasite-type $IrTe_2$
SG: $Pnnm$, $a = 5.5381$ Å, $b = 6.5138$ Å, $c = 4.1398$ Å, $V = 149.34$ Å^3
Atom coordinates: Ir (0, 0, 0); Te (0.2285, 0.3665, 0)

[a] The experimental values are given in italics in parentheses.

phases calculated by EHTB calculations using the crystal structures determined by VASP calculations are presented in Figs. 2a–2g.

3. RELATIVE STABILITIES OF VARIOUS $IrTe_2$ PHASES

As compared in Tables 1a–1c, the cell parameters and the atom positions of the three experimentally known $IrTe_2$ phases are well reproduced by the VASP calculations (with less than 2% difference). The relative stabilities of the $IrTe_2$ phases (based only on our calculations of the internal energies at 0 K) increase in the order

TABLE 2
Relative Energies (eV) and Cell Volumes (Å^3) per Formula Unit Determined by VASP Calculations for Some Observed and Hypothetical $IrTe_2$ Phases

Phase	Relative energy	Cell volume
Monoclinic[a]	0.000	74.18
IrS_2-type[b]	0.015	75.79
Ramsdelite-type[b]	0.049	75.94
CdI_2-type[a]	0·094	75·47
Pyrite-type[a]	0.217	70.41
Marcasite[b]	0.219	74.67
Pyrolusite[b]	0.884	79.39

[a] Observed.
[b] Hypothetical.

TABLE 3
Gross Populations of the Ir 5*d* and Te 5*p* Orbitals and Charge Balance of Various $IrTe_2$ Phases Obtained by EHTB Calculations

Phase type	Ir 5*d*	Te 5*p*	Charge balance
CdI_2	7.92	4.03	$(Ir^{3+})(Te^{1.5-})_2$
Monoclinic	8.11/Ir(1)	3.72/Te(1)	$(Ir^{3+})_3(Te_2)^{2-}(Te^{1.75-})_4$
	7.93/Ir(2)	4.04/ Te(2)	
		4.15/Te(3)	
Pyrite	8.30	3.86	$(Ir^{2+})(Te_2)^{2-}$
Pyrolusite	7.61	4.24	$(Ir^{4+})(Te^{2-})_2$
Marcasite	8.30	3.85	$(Ir^{2+})(Te_2)^{2-}$
IrS_2	7.99/Ir(1)	3.71/Te(1)	$(Ir^{3+})_3(Te^{2-})_3(Te_2^{2-})_{3/2}$
	7.93/Ir(2)	4.42/Te(2)	
		3.68/Te(3)	
		4.31/Te(4)	
Ramsdelite	7.98	4.00/Te(1)	$(Ir^{3+})(Te^{1.5-})_2$
		4.01/Te(2)	

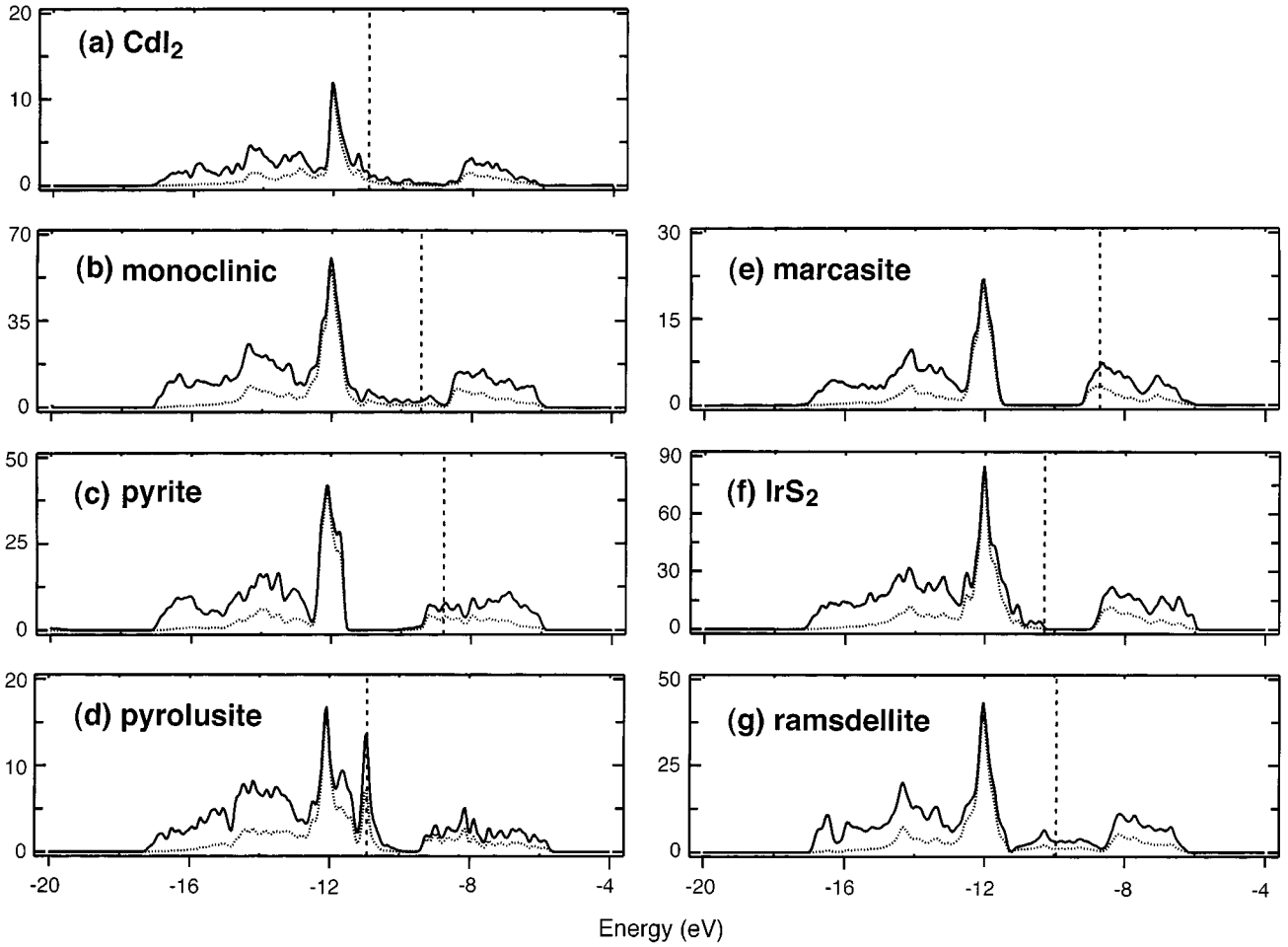

FIG. 2. Plots of the density of states calculated for some observed and hypothetical $IrTe_2$ phases using the EHTB method: (a) the polymeric CdI_2-type phase, (b) the monoclinic phase, (c) the pyrite-type phase, (d) the pyrolusite-type phase, (e) the marcasite-type phase, (f) the IrS_2-type phase, and (g) the ramsdelite-type phase. The vertical dashed lines refer to the Fermi levels. Each unit cell has one formula unit (FU) in the polymeric CdI_2-type phase, two FUs in the pyrolusite- and marcasite-type phases, four FUs in the pyrite- and ramsdelite-type phases, six FUs in the monoclinic phase, and eight FUs in the IrS_2-type phase. In each plot the vertical axis refers to the number of electrons per unit cell, the solid line to the total density of states, and the dotted line to the projected density of states for the Ir5*d* orbitals.

pyrolusite-type < marcasite-type < pyrite-type < polymeric CdI_2-type < ramsdelite-type < IrS_2-type < monoclinic. The unit cell volume per formula unit $IrTe_2$ increases in the order pyrite-type < monoclinic < marcasite-type < polymeric CdI_2-type < IrS_2-type < ramsdelite-type < pyrolusite-type (see Table 2 and Scheme 1). Based on these findings, we discuss the feasibility of preparing $IrTe_2$ phases under pressure. (Here it should be pointed out that the polymeric CdI_2 form is predicted to be less stable than the ramsdelite-, IrS_2-, and monoclinic-type phases. This prediction is incorrect because the polymeric CdI_2 form is the preferred product under high temperature and ambient pressure. In general, first-principle calculations based on density functional theory do not treat layered compounds properly because their van der Waals gaps have low electron density.

The cell volume of the pyrite-type phases is smaller than that of the monoclinic $IrTe_2$, which in turn is smaller than

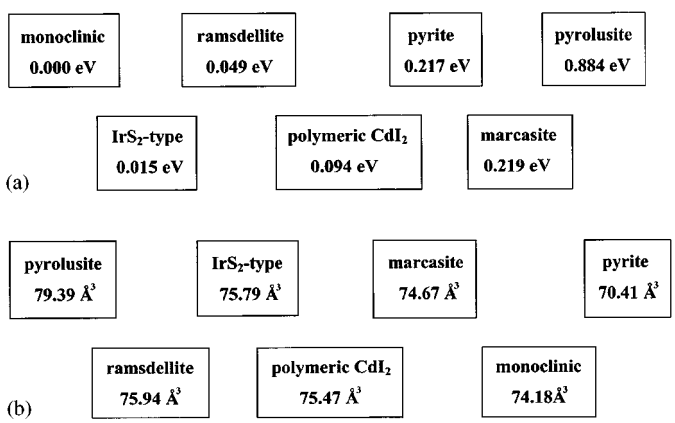

SCHEME 1. Relative energies and unit cell volumes of some $IrTe_2$ phases. (a) Relative energies per formula unit. (b) Unit cell volume per formula unit.

that the polymeric CdI_2-type phase. This is consistent with the experimental observation that the polymeric CdI_2-type phase is converted to the monoclinic phase under pressure (5 GPa) and to the pyrite-type phase under higher pressure (20 GPa) at room temperature. The pyrolusite-type phase has the largest cell volume and is least stable energetically (Table 2 and Scheme 1), so it should not be possible to prepare this phase under high pressure. Furthermore, the charge balance of this hypothetical $IrTe_2$ from implies the occurrence of Ir^{4+} and Te^{2-} (see below), which is unrealistic since tellurium cannot oxidize iridium to this high oxidation state.

The ramsdelite- and IrS_2-type phases are calculated to be more stable than the polymeric CdI_2-type phase for the reasons mentioned above. Nevertheless, the ramsdelite- and the IrS_2-type phases would be chemically stable in view of the fact that they possess similar building blocks as does the monoclinic $IrTe_2$, and that they only exhibit a slightly higher total energy. However, the ramsdelite- and the IrS_2-type forms have cell volumes much larger than that of m-$IrTe_2$ (75.94 and 75.79 $Å^3$ versus 74.18 $Å^3$). Consequently, the stabilities of the ramsdelite- and the IrS_2-type phases should decrease under pressure.

There are only three $IrTe_2$ phases that have a cell volume smaller than that of the polymeric CdI_2-type phase, i.e., monoclinic, pyrite-type, and marcasite-type phases. The monoclinic and pyrite-type $IrTe_2$ phases have already been synthesized under pressure. The marcasite-type phase is similar in relative stability to the pyrite-type phase and has a cell volume slightly larger than that of the monoclinic phase (by 0.49 $Å^3$/formula unit) (Scheme 1). Thus, considering only the cell volume criterion, one might suggest that preparation of the marcasite-type $IrTe_2$ phase under pressure is feasible, and that pressures lower than about 5 GPa would be desirable for the synthesis of the marcasite-type Ir/Te_2 because it has a cell volume slightly larger than that of the monoclinic $IrTe_2$ form. Nevertheless, synthesis of the marcasite-type $IrTe_2$ would be difficult for the following reasons: (1) The monoclinic and marcasite-type $IrTe_2$ phases have very similar cell volumes (per formula unit), and the monoclinic form is considerably more stable than the marcasite form (Table 2), so that synthesis under pressure lower than 5 GPa might favor the formation of the monoclinic $IrTe_2$ rather than that of the marcasite-type $IrTe_2$. (2) The marcasite- and pyrite-type $IrTe_2$ phases are practically the same in stability, but the pyrite-type form has a considerably smaller cell volume. Thus an attempt to prepare the marcasite-type $IrTe_2$ under pressure higher than 5 GPa might preferentially lead to the pyrite-type $IrTe_2$.

4. CHARGE BALANCE AND UNIT CELL VOLUME

The charge balances of the polymeric CdI_2-, monoclinic, and pyrite-type $IrTe_2$ phases are best described by $(Ir^{3+})(Te^{1.5-})_2$, $(Ir^{3+})_3(Te_2)^{2-}(Te^{1.75-})_4$, and $Ir^{2+}(Te_2)^{2-}$, respectively (12). These oxidation states assignments are consistent with the trends in the gross populations of the Ir 5*d* and Te 5*p* orbitals listed in Table 3. The pyrolusite-type phase has the smallest Ir 5*d* gross population and the largest Te 5*p* gross population. The charge balance of the pyrolusite-type phase can be approximated as $(Ir^{4+})(Te^{2-})_2$, which is consistent with the DOS plot of Fig. 2d, where the Fermi level lies in the lower-lying *d*-block bands. The structural change from the pyrolusite-type to the marcasite-type phase produces short Te ⋯ Te contacts (3.070 Å) that leads to a Te-5*p* → Ir-5*d* charge transfer. The Ir-5*d* and Te-5*p* orbital gross populations of the marcasite-type phase become very similar to those of the pyrite-type phase. Consequently, the charge balance of the marcasite-type phase should be close to that of the pyrite-type phase, i.e., $(Ir^{2+})(Te_2)^{2-}$. The similarities between the DOS plots of the pyrite- and marcasite-type phases support this point (Figs. 2c and 2e). Recall that the calculated stabilities of the pyrite- and marcasite-type $IrTe_2$ phases are quite similar (Table 2). Nevertheless, the pyrite-type form has been observed while the marcasite-type has not. As can be seen from the cell volume per formula unit (70.41 versus 74.67 $Å^3$), this reflects the fact that the pyrite-type form is considerably more compact than the marcasite-type form. The Ir-5*d* and Te-5*p* orbital gross populations of the ramsdelite-type phase are very similar to those of the polymeric CdI_2-type phase (Table 3), so that the charge balance of the ramsdelite-type phase should also be $(Ir^{3+})(Te^{1.5-})_2$. As expected, therefore, the DOS plots of the polymeric CdI_2-type and ramsdelite-type phases are similar (Figs. 2a and 2g). A unit cell of the IrS_2-type phase contains four $IrTe_4$ single-octahedral chains and two Ir_2Te_6 double-octahedral chains (Fig. 1f), so that three short Te ⋯ Te contacts (Te(1) ⋯ Te(3) = 2.946 Å) are present in a unit cell. To a first approximation, these short Te ⋯ Te contacts should be described as Te_2^{2-} dimers since they are shorter than the Te_2 pair bond distances of pyrite-type phases, and their overlap population is greater than the corresponding value of the pyrite-type phase. Thus the charge balance of the IrS_2-type $IrTe_2$ can be described as $(Ir^{3+})_3(Te^{2-})_3(Te_2^{2-})_{3/2}$. The DOS plot Fig. 2f shows that the IrS_2-type phase is a semiconductor unlike the other $IrTe_2$ phases, which are metallic.

The charge balances appropriate for the various $IrTe_2$ phases are summarized in Table 3. Comparisons between the charge balances and the unit cell volumes indicate that the cell volume generally increases as the average negative charge on Te increases. Therefore, if the marcasite-type phase is excluded from comparison, it is found that the pyrolusite-type phase has the largest cell volume with the average charge − 2 on Te, and the pyrite-type phase has the smallest cell volume with the average charge − 1 on Te. The remaining four phases have the average charge − 1.5 on Te and possess a cell volume that lies between the

cell volume of the pyrite- and that of the pyrolusite-type phase. Note that the Ir–Te distances (determined from first principles calculations) vary only in the limited range of 2.631–2.775 Å for the seven calculated $IrTe_2$ forms. This feature, which is in agreement with the available experimental results (9, 11, 12), indicates that the Ir–Te distance do not strongly depend on the oxidation state of Ir.

5. CONCLUDING REMARKS

The present study correctly predicts that preparation of the monoclinic and pyrite-type $IrTe_2$ phases is favorable under pressure. On the basis of the energy, the cell volume, and the oxidation state, one can definitely rule out the possibility of preparing the pyrolusite-type $IrTe_2$. Although the IrS_2- and ramsdelite-type $IrTe_2$ phases are only slightly higher in energy than the monoclinic $IrTe_2$, their unit cell volumes (per formula unit) are much larger than that of the monoclinic $IrTe_2$. Thus the IrS_2- and ramsdelite-type $IrTe_2$ phases would be difficult to prepare under pressure, because high-pressure synthesis must favor the formation of the monoclinic $IrTe_2$. In contrast, the pyrite-, monoclinic-, and marcasite-type $IrTe_2$ phases possess a unit cell volume (per formula unit) smaller than that of the CdI_2-type $IrTe_2$. According to the cell-volume criterion alone, the preparation of the marcasite-type $IrTe_2$ under pressure appears feasible. However, under synthetic conditions favorable for the formation of the marcasite-type $IrTe_2$, the monoclinic or the pyrite-type $IrTe_2$ would be formed preferentially. In discussing possible phases attainable under pressure it is important to consider both the energy and the cell volume.

ACKNOWLEDGMENTS

The work at North Carolina State University was supported by the Office of Basic Energy Sciences, Division of Materials Sciences, U.S. Department of Energy, under Grant DE-FG05-86ER45259.

REFERENCES

1. C. F. van Bruggen, *Ann. Chim. Fr.* **7,** 171 (1982).
2. S. Jobic, R. Brec, and J. Rouxel, *J. Solid State Chem.* **96,** 169 (1992).
3. S. Jobic, R. Brec, and J. Rouxel, *J. Alloys Compd.* **178,** 253 (1992).
4. J. Rouxel, *Comments Inorg. Chem.* **14,** 207 (1992).
5. E. Canadell, S. Jobic, R. Brec, J. Rouxel, and M.-H. Whangbo, *J. Solid State Chem.* **89,** 189 (1992).
6. M.-H. Whangbo and E. Canadell, *J. Am. Chem. Soc.* **114,** 9587 (1992).
7. P. Alemany, S. Jobic, R. Brec, and E. Canadell, *Inorg. Chem.* **36,** 5050 (1997).
8. P. Alemany and E. Canadell, *Eur. J. Inorg. Chem.* **10,** 1701 (1999).
9. S. Jobic, P. Deniard, R. Brec, J. Rouxel, A. Jouanneaux, and A. N. Fitch, *Z. Anorg. Allg. Chem.* **598/599,** 199 (1991).
10. E. F. Hocking and J. G. White, *J. Phys. Chem.* **64,** 1042 (1960).
11. J.-M. Léger, A. S. Periera, J. Haines, S. Jobic, and R. Brec, *J. Phys. Chem. Solid* **61,** 27 (2000).
12. S. Jobic, R. Brec, C. Château, J. Haines, J.-M. Léger, H.-J. Koo, and M.-H. Whangbo, *Inorg. Chem.* **39,** 4370 (2000).
13. A. F. Wells, "Structural Inorganic Chemistry." Oxford Univ. Press, Oxford, 1962.
14. L. B. Barricelli, *Acta Crystallogr.* **11,** 75 (1958).
15. S. Jobic, P. Deniard, R. Brec, J. Rouxel, M. G. B. Drew, and W. I. F. David, *J. Solid State Chem.* **89,** 315 (1999).
16. G. Kresse and J. Hafner, *Phys Rev. B.* **47,** 558 (1993).
17. L. Magaud, A. Pasturel, G. Kresse, and J. Hafner, *Phys. Rev. B* **55,** 13,479 (1997).
18. G. Kresse and J. Furthmüller, *Comput Sci.* **6,** 15 (1996).
19. G. Kresse and J. Furthmüller, *J. Phys. Rev. B* **54,** 11,169 (1996).
20. G. Kresse and J. Hafner, *J. Phys.: Condens. Matter* **6,** 8245 (1994).
21. D. Vanderbilt, *Phys. Rev. B.* **41,** 7892 (1991).
22. J. P. Perdew and Y. Wang, *Phys. Rev. B* **33,** 8800 (1986).
23. M.-H. Whangbo and R. Hoffman, *J. Am. Chem. Soc.* **100,** 6397 (1978).
24. Our calculations were carried out by employing the *CAESAR* program package (Ren, J., Liang, W. and Whangbo, M.-H., *Crystal and electronic structure analysis using CAESAR*, 1998, available at http://www.PrimeC.com/.)